nature physics

SUPPLEMENTARY INFORMATION

DOI: 10.1038/NPHYS2012

# Dynamical *d*-wave condensation of exciton-polaritons in a two-dimensional square-lattice potential

Na Young Kim[1,2], Kenichiro Kusudo[3], Congjun Wu[4], Naoyuki Masumoto[3], Andreas Löffler[5], Sven Höfling[5], Norio Kumada[6], Lukas Worschech[5], Alfred Forchel[5] & Yoshihisa Yamamoto[1,3]

***Summary***

We explicitly describe the theoretical method to compute the band structure of a single particle in a two-dimensional square lattice potential. We also present a simple model using coupled rate equation to describe the dynamics and the mode competition. Both near-field wavefunction and far-field population distribution are computed in the case of a strong lattice potential with a 3-by-3 site as a comparison to our weak potential case presented in the main text.

***Band structure of a two-dimensional square lattice potential***

We solve the single particle Schrödinger equation with an effective lower polariton mass, $m^*$, $-\frac{\hbar^2}{2m^*}\nabla^2\Psi(\vec{r})+V(\vec{r})\Psi(\vec{r})=E\Psi(\vec{r})$. $V$ represents a two-dimensional periodic potential: $V(\vec{r})=\sum_i g(r-\vec{R}_i)$, where $\vec{R}_i$ is the location of lattice site center and g(r) is the potential of circular wells with radius $r_0$ ,

$$g(\vec{r})=\begin{cases}-V_0 & for\ \ r<r_0\\ 0 & for\ \ r>r_0\end{cases},$$

$V_0$ is the potential depth, and $a$ is the lattice constant. In our experiment system, $a$ = 4 μm, and $r_0$ = 2 μm. The characteristic energy scale is defined as $E_0=\frac{\hbar^2}{2m^*}\left|\frac{2\pi}{a}\right|^2 \sim 1$

DOI: 10.1038/NPHYS2012

meV with the first Brillouin zone edge, $2\pi / a$. Experimentally we have found that the potential strength is ~ 200 μeV, which corresponds to $V_0 = 0.2\ E_0$.

We employ the standard method using the plane wave basis for this weak periodic potential lattice. The general reciprocal lattice vectors $\vec{G}_{mn} = m\vec{b}_1 + n\vec{b}_2$ (m, n are integers) are represented in terms of the reciprocal lattice vector bases, $\vec{b}_1 = \left(\frac{2\pi}{a},\ 0\right)$ and $\vec{b}_2 = \left(0,\ \frac{2\pi}{a}\right)$. The plane basis is denoted as $\left|\vec{k} + \vec{G}_{mn}\right\rangle$, where the plane wave wavevector $\vec{k}$ is limited within the first Brillouin zone. The Hamiltonian operator, $\hat{H} = -\frac{\hbar^2}{2m^*}\hat{k}^2 + \hat{V}(x, y)$, is expressed in a matrix form by computing $\left\langle \vec{k} + \vec{G}_{mn} \middle| \hat{H} \middle| \vec{k} + \vec{G}_{mn} \right\rangle$ and diagonalized. Along the three high-symmetry points, *Γ, X* and *M* in a reciprocal lattice space, the band structure is computed with $V_0 = 0.2\ E_0$ shown in Fig. 1**b** in the main text.

At the high symmetry points *Γ*, *X* and *M*, the weak lattice potential lifts the degeneracy of the Bloch eigenstates according to their properties under the four-fold lattice symmetry transformation. For example, at the *M* point, the lowest nearly degenerate four Bloch eigenstates transform according to the s-, $p_x$-, $p_y$-, $d_{xy}$-symmetries, respectively. The values of the band gap energy are determined by the potential strength and they are in the range between 4 – 40 % of $V_0$ depending on their symmetry indices.

***Near-field and far-field wavefunctions in a strong potential lattice***

In the case of the strong lattice potential, the Bloch wave band eigenstates can be studied from the tight-binding model. Energy levels with different orbital symmetry indicdes (e.g., *s*, $p_x$, $p_y$, $d_{xy}$) inside one lattice site is broadened into orbital energy bands. At the high symmetry points in the Brillouin zone, these orbital symmetry indices play the same role of the point-group symmetry indices in the weak-coupling potential.

Below we present an illustration of the orbital symmetry of condensate wavefunction in the strong lattice from the perspective of orbital energy bands.

The orbital symmetry of near-field wavefunctions in a square lattice is readily captured in the case of the strong parabolic trap potential due to the localization of wavefunctions per each site. Figure S1 shows the near-field wavefunctions and far-field intensities formed by a 3-by-3 square lattice array with an individual strong parabolic potential profile. It is also clearly seen the in-phase and anti-phase arrangement of wavefunction between sites. Namely, both $p_x$- and $d$-orbital wavefunctions are $\pi$-phase shifted with respect to the nearest neighbour site. With these near-field wavefunctions, the far-field intensities are calculated by taking Fourier transform. Since the finite lattice array and the localization, there are stronger side peaks beyond the first Brillouin zones unlike the case of the weak potential lattice in Fig. 3.

***Dynamics and mode competition***

The dynamics of the preferred orbital states can be easily explained by the simple rate equations with the population of four states: (1) the reservoir exciton-polaritons injected by the pump laser, $n_p$, (2) the s-wave ground state $n_\Gamma$ at $\Gamma$, (3) the $p_x$-wave state $n_X$ at $X$, and (4) the $d$-wave state, $n_M$ at $M$. We introduced the radiative decay rate $\Gamma_i$, of the state i and the transition rate $\Gamma_{ij}$ from i-state to j state. The four coupled rate equations are set up as:

$$\frac{dn_p(t)}{dt} = -\Gamma_p n_p - \Gamma_{pM} n_p (n_M + 1) - \Gamma_{pX} n_p (n_X + 1) - \Gamma_{p\Gamma} n_p (n_\Gamma + 1),$$

$$\frac{dn_M(t)}{dt} = -\Gamma_M n_M + \Gamma_{pM} n_p (n_M + 1) - \Gamma_{MX} n_M (n_X + 1) - \Gamma_{M\Gamma} n_M (n_\Gamma + 1),$$

$$\frac{dn_X(t)}{dt} = -\Gamma_X n_X + \Gamma_{pX} n_p (n_X + 1) + \Gamma_{MX} n_M (n_X + 1) - \Gamma_{X\Gamma} n_X (n_\Gamma + 1),$$

$$\frac{dn_\Gamma(t)}{dt} = -\Gamma_\Gamma n_\Gamma + \Gamma_{p\Gamma} n_p (n_\Gamma + 1) + \Gamma_{M\Gamma} n_M (n_\Gamma + 1) + \Gamma_{X\Gamma} n_X (n_\Gamma + 1).$$

DOI: 10.1038/NPHYS2012

From the phenomenological behaviour measured in experiments, we choose the following numerical values for the decay rate and the transition rates: $\Gamma_p = 1/300$ ($ps^{-1}$), $\Gamma_M = 1/10$ ($ps^{-1}$), $\Gamma_X = 1/10$ ($ps^{-1}$), $\Gamma_\Gamma = 1/5$ ($ps^{-1}$), $\Gamma_{pM} = 1/20$ ($ps^{-1}$), $\Gamma_{pX} = 1/100$ ($ps^{-1}$), $\Gamma_{p\Gamma} = 1/100$ ($ps^{-1}$), $\Gamma_{MX} = 1/20$ ($ps^{-1}$), $\Gamma_{M\Gamma} = 1/100$ ($ps^{-1}$), and $\Gamma_{X\Gamma} = 1/40$ ($ps^{-1}$). The obtained result is presented in Fig. 2**b**.

Supplement Figure 1.

**Figure S1. Theoretical near-field (NF) and far-field (FF) patterns in a weak potential**. The calculation is performed using single-particle plane-wave bases in a weak periodic lattice potential, and the NF (up panel) wavefunctions and FF intensity distributions (bottom panel) for the 1*s* (**a**), $2p_x$ (**b**), $3d_{xy}$ (**c**) -orbital condensates are presented, where the white (violate) color indicates positive (negative) amplitudes in real space wavefunctions and the red (blue) color indicates high (low) positive intensity values in momentum space. The positions of circular traps (apertures) on the device surface are drawn with black circles by the removed background color. Whereas 1*s*-orbital wavefunctions are connected in-phase between lattice sites, both $2p_x$, $3d_{xy}$ wavefunctions are connected with anti-phased manner. The anti-phased $2p_x$, $3d_{xy}$ wavefunctions in real space induce interference peaks at *X* and *M* points, respectively, in the momentum space. The relatively delocalized wavefunctions over a shallow potential landscape in the finite size lattice exhibit only the first-order interference peaks in comparison to the significant multiple-side peaks in the FF patterns for strong parabolic trap cases in Fig. 3.

Supplement Figure S2.

**Figure S2. Energy-momentum dispersion characteristics.** The cross-sectional energy-momentum dispersion relations are measured at $P/P_{th} = 1$ ($P_{th} = 7$ mW) (**a**) and

$P/P_{th} \sim 7$ (**b**), along the line 3 indicated in (**c**). It provides the energy values and the population of $2p_x$ condensate states.

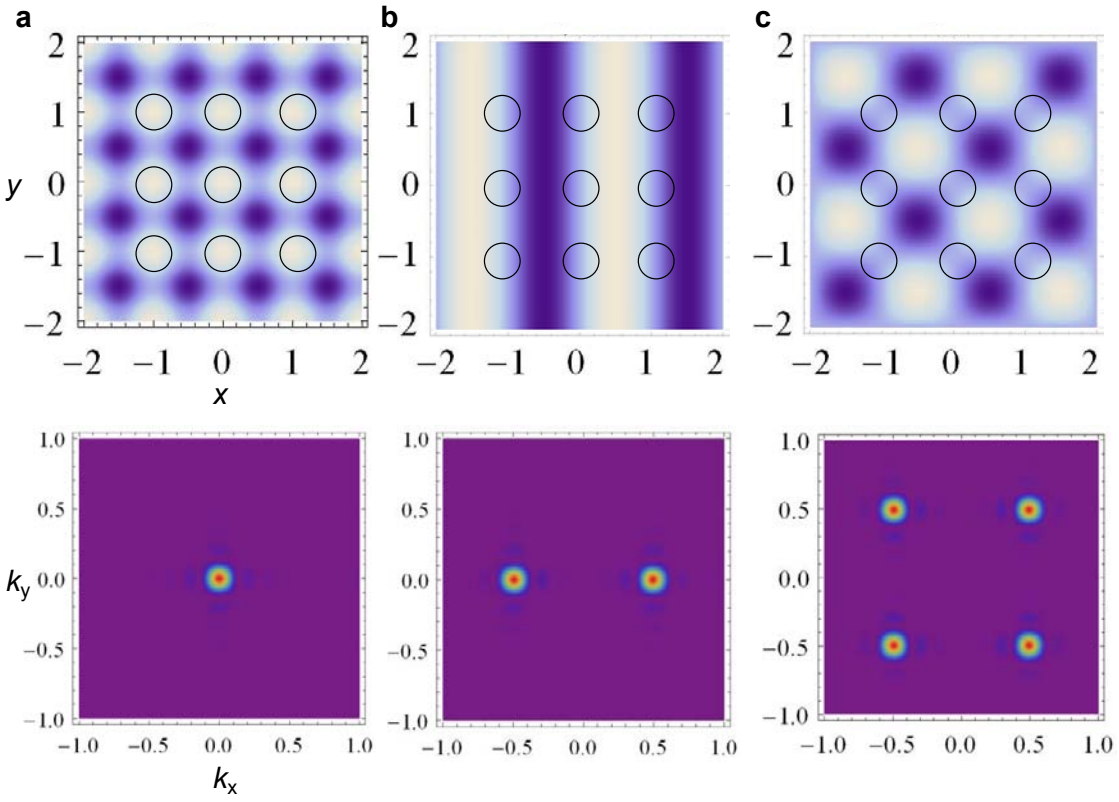


**Supplement Figure S1**

DOI: 10.1038/NPHYS2012

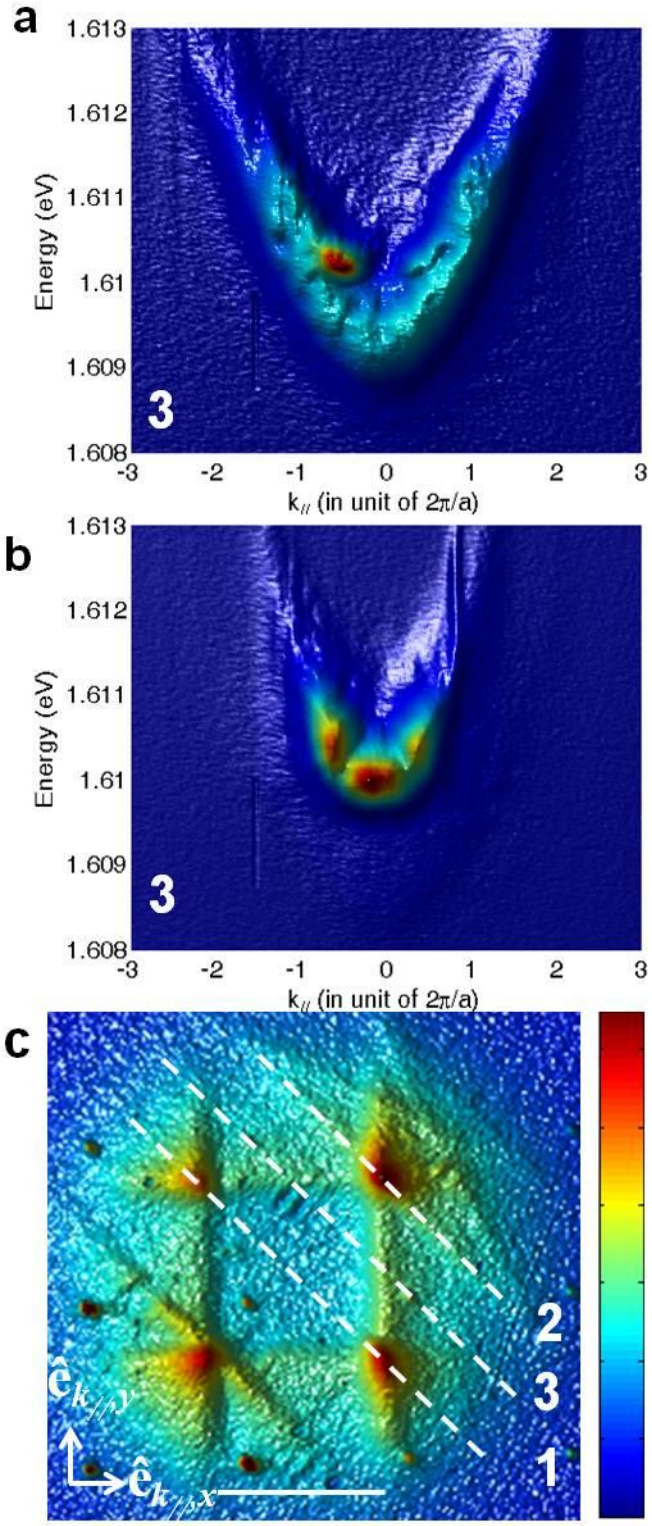


**Supplement Figure S2**